NANOSCALE CHARACTERIZATION OF SOLUTION-CAST POLY(VINYLIDENE FLUORIDE) THINFILMS USING ATOMIC FORCE MICROSCOPY

A Thesis

by

TAE KWON JEE

Submitted to the Office of Graduate Studies of
Texas A&M University
in partial fulfillment of the requirements for the degree of

MASTER OF SCIENCE

December 2005

Major Subject: Mechanical Engineering

NANOSCALE CHARACTERIZATION OF SOLUTION-CAST POLY(VINYLIDENE FLUORIDE) THINFILMS USING ATOMIC FORCE MICROSCOPY

A Thesis

by

TAE KWON JEE

Submitted to the Office of Graduate Studies of
Texas A&M University
in partial fulfillment of the requirements for the degree of

MASTER OF SCIENCE

Approved by:

Chair of Committee,	Hong Liang
Committee Members,	Debjyoti Banerjee
	Sunil Khatri
Head of Department,	Dennis O' Neal

December 2005

Major Subject: Mechanical Engineering

ABSTRACT

Nanoscale Characterization of Solution-Cast Poly(Vinylidene Fluoride) Thinfilms Using Atomic Force Microscopy.

(December 2005)

Tae Kwon Jee, B.S., Hanyang University, Seoul, Korea

Chair of Advisory Committee: Dr. Hong Liang

This thesis research focuses on the characterization of thinfilms made of poly(vinylidene fluoride) (PVDF) using an atomic force microscope. Thinfilms of PVDF were fabricated by a spin coating method with different conditions and characterized using the Atomic Force Microscopy (AFM) for morphological changes. Phase and conformational changes of PVDF were investigated using both wide angle X-ray diffraction (WAXD) and Fourier Transform Infrared Spectroscopy (FTIR). From this analysis, in-situ corona poling with annealing of spin-cast PVDF enabled a phase change from α to the mixture of β and γ phases. This process can decrease the complexity of the conventional method which requires mechanical stretching before poling PVDF in addition to thermal annealing for β phase transformation. This thesis describes some materials and surface properties of solution-cast PVDF thinfilms with various conditions such as topography and phase image, adhesion force, friction force, and roughness. Through the AFM topography and phase images, polymeric behavior and spherulites are discussed in the later part of the thesis.

DEDICATION

.

To My Wife, My Son, My Parents, and All My Dearest Friends, and Especially, Jesus, My God, Who Makes My Dreams Come True

ACKNOWLEDGEMENTS

I would like to thank my committee chair, Dr. Hong Liang, and my committee members, Dr. Debjyoti Banerjee and Dr. Sunil Khatri, for their guidance, support, and encouragement throughout this research. Thanks also to my friends, especially Ted Eisenbach and my colleagues in the surface science laboratory, who helped my research in many different ways. Acknowledgements extend to the Mechanical Engineering Department faculty and staff at the Texas A&M University for helping me to get the good engineering sense and knowledge, and for making me a good engineer. I appreciate the financial support from the National Science Foundation (IIS-0515930), for providing funding for my research. I also thank all the members of Vision Mission Church and Korean Student Association who were willing to pray for me. Finally, thanks to my mother, father, and parents-in-law for their encouragement, and to my wife and son for their patience and love, especially, Jesus, my god, who makes my dreams come true.

TABLE OF CONTENTS

CHAPTER Page

LIST OF FIGURES

FIGURE Page

LIST OF TABLES

NOMENCLATURE

PVDF	Poly(Vinylidene Fluoride)
AFM	Atomic Force Microscope
LFM	Lateral Force Microscopy
STM	Scanning Tunneling Microscopy
EFM	Electrostatic Force Microscopy
WAXD	Wide Angle X-ray Diffraction
FTIR	Fourier Transform Infrared Spectroscopy
X	Stress
x	Strain
g_{ij}	Piezoelectric Coefficient
d_{ij}	Inverse Piezoelectric Coefficient
E	Electric Field
D	Electric Displacement
c	Elastic Constant
ε	Dielectric Constant
ε_0	Permittivity of Vacuum
e	Piezoelectric Tensor
κ	Permittivity Tensor
TG^+TG^-	α and δ Phases

TTT	β Phase
$T_3G^+T_3G^-$	γ and ε Phases
HMPA	Hexamethylphoramide
DMSO	Dimethylsulphoxide
DMF	Dimethyl-formamide
DMAc	Dimethylacetamide
$CH_2 = CF_2$	Repeated Monomer Unit of PVDF
n	Order of a Reflection
λ	Wavelength of X-ray
d	Distance between Parallel Lattice Planes
θ	Angle between the Incident Beam and a Lattice Plane
k	Force Constant
μ	$m_1\, m_2/(m_1+m_2)$
c	Velocity of Light
Rpm	Revolve per Minute
CMP	Chemical Mechanical Planarization

CHAPTER I

INTRODUCTION

1.1. History and Background

1.1.1. Discovery of the Piezoelectric Effect

In 1756, Aepinus noticed the opposite polarities between two ends of a heated tourmaline crystal, and he proved the electrical nature of this phenomenon.[1] In 1880, brothers Pierre and Jacques Curie discovered the direct piezoelectric effect, and announced their experiments at the session of the Académie des Sciences in Paris.[1-3] For more than 30 years from the discovery of brothers Curie, however, this effect was not applied to the practical problems but only scientific curiosity. During World War II, Langevin contrived the sonar system from converse piezoelectric effect using exciting quartz plate.[1] The ultrasonic waves bounced back by object in the water could be captured again by the quartz plate. Nowadays, there are many industrial applications through this piezo- or inverse piezoelectric effect such as transducers, sensors, actuators, power generators, piezo motors, and even fuel cells.[1, 4-7]

1.1.2. Brief Overview of Piezoelectricity

The word "piezo" means press from Greek "piezin" and piezoelectricity is the ability of certain crystals to generate a voltage in response to applied mechanical stress by definition of encyclopedia. The electric signal can be measured as a charge flow from one electrode surface to the other across the piezo-materials. The electrical response of

---

This thesis follows the style of the *Journal of the Electrochemical Society.*

piezo-materials is functions of both stress(X) applied to the electrode area and the mechanical strain(x) that the material experiences. We can define the piezoelectric coefficient(g_{ij}) and inverse piezoelectric coefficient(d_{ij}) by following partial differential equations.[2-4]

$$d = \left(\frac{\partial D}{\partial X} \right)_{E=0} \tag{1}$$

$$g = \left(\frac{\partial E}{\partial X} \right)_{D=0} \tag{2}$$

$$e = \left(\frac{\partial D}{\partial x} \right)_{E=0} \tag{3}$$

$$h = \left(\frac{\partial E}{\partial x} \right)_{D=0} \tag{4}$$

where open circuit change is labeled in [E], electric field in [V/m], short circuit change in [D], the electric displacement [m]. Coefficients are related to each other because the stress and strain in each element and the electrical displacement and field are governed by elastic constant(c) and the dielectric constant(ε), respectively.

$$c = \frac{e}{d} = \frac{h}{g} \tag{5}$$

$$\varepsilon\varepsilon_0 = \frac{d}{g} = \frac{e}{h} \tag{6}$$

where ε_0 is the permittivity of vacuum. The piezoelectric response can make material's stiffness increase because the strain causes both stress and polarization. The polarization increases the inner stress by relation " $X_{polarization}$ = eE". So, the total stress is

$$X_{ij} = X_{strain} + X_{polarization} = c_{ijmn} x_{mn} + e_{nij} E_n \tag{7}$$

Similarly,

$$D_{ij} = D_{strain} - D_{polarization} = e_{imn} x_{mn} - \kappa_{ij} E_n \tag{8}$$

where X is the stress tensor, x is strain tensor, E is electric field vector, and D, c, e, and κ are electric displacement vector, the elastic stiffness tensor, the piezoelectric tensor, and the permittivity tensor, respectively. We can express these coefficients and relationships as a matrix using above formulas (1)-(8). The constitutive equation of piezoelectric material is

$$\begin{bmatrix} X_{11} \\ X_{22} \\ X_{33} \\ X_{23} \\ X_{13} \\ X_{12} \\ \hline D_1 \\ D_2 \\ D_3 \end{bmatrix} = \left[\begin{array}{cccccc|ccc} C_{11} & C_{12} & C_{13} & 0 & 0 & 0 & 0 & 0 & e_{31} \\ C_{12} & C_{22} & C_{23} & 0 & 0 & 0 & 0 & 0 & e_{32} \\ C_{13} & C_{23} & C_{33} & 0 & 0 & 0 & 0 & 0 & e_{33} \\ 0 & 0 & 0 & C_{44} & 0 & 0 & 0 & e_{24} & 0 \\ 0 & 0 & 0 & 0 & C_{55} & 0 & e_{15} & 0 & 0 \\ 0 & 0 & 0 & 0 & 0 & C_{66} & 0 & 0 & 0 \\ \hline 0 & 0 & 0 & 0 & e_{15} & 0 & -\kappa_1 & 0 & 0 \\ 0 & 0 & 0 & e_{24} & 0 & 0 & 0 & -\kappa_2 & 0 \\ e_{31} & e_{32} & e_{33} & 0 & 0 & 0 & 0 & 0 & -\kappa_3 \end{array}\right] \begin{bmatrix} x_{11} \\ x_{22} \\ x_{33} \\ x_{23} \\ x_{13} \\ x_{12} \\ \hline E_1 \\ E_2 \\ E_3 \end{bmatrix} \tag{9}$$

Considering the piezoelectric polymer, poly(vinilydene fluoride), mechanical anisotropy can be caused by stretching the films during manufacturing process as well as aligning dipoles preferentially in the direction of the poling field during poling process. As one can see in Figure 1, the '1' is the stretching direction and '3' is the net dipole direction. We will also get the stretching direction at '2' axis if the film undergo biaxial stretching. In case of uniaxial orientation, '2' direction is normal to the machine

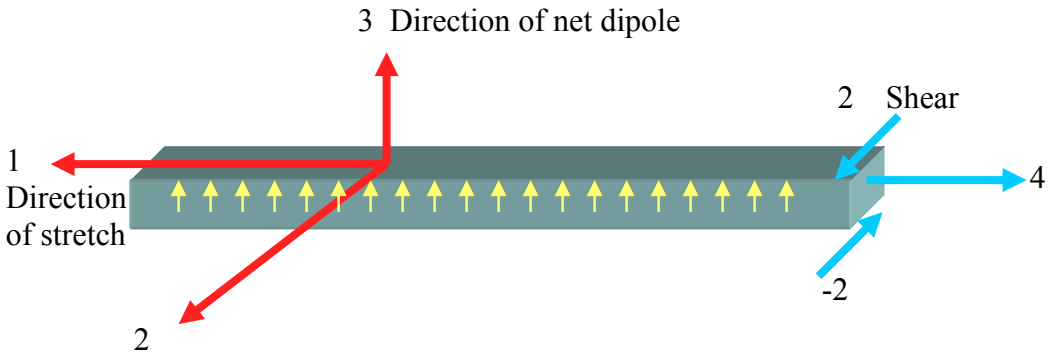

Figure 1 Schematic diagram of polymer thin film.

direction and dipole direction. The piezoelectric strain coefficient, d_{ij} , can be expressed with tensor notation.

$$d_{ij} = \begin{bmatrix} 0 & 0 & 0 & 0 & d_{15} & 0 \\ 0 & 0 & 0 & d_{24} & 0 & 0 \\ d_{31} & d_{32} & d_{33} & 0 & 0 & 0 \end{bmatrix} \tag{10}$$

As we know from Figure 1, net dipole can only exist in the direction of 3, thus, 1 and 2 have no charge due to the uniaxial deformation. Tensile stress is considered positive, but the polarization will decrease as the film thickness increases. The notes d_{3j} are the most important components for producing piezoelectricity. The positive deformation in 1 or 2 direction can cause a decrease in film thickness, and will give positive charge to 3 direction. Shear stress 4 and 5 will cause a rotation about the axis 1 and 2, respectively. Therefore, they give some values, but all j=6 components are zero because of no stress on the 3 axis.

1.1.3. Piezoelectric Polymers

Due to their high pyro-, and piezoelectric properties, poly(vinylidene fluoride) (PVDF) is a widely studied polymer and is of great importance in many engineering applications.[2-4,8] Besides high piezoelectric coefficient, their advantages such as flexibility, bio-compatibility, lightness, and low acoustic and mechanical impedance make PVDF a favorable material for bio- and MEMS applications. Although solution casting method for making a PVDF thin film is simple and cost-effective, there is less use in industry because of the difficulty getting β phase which has the best piezoelectric response among 4 major types of polymorph: TG^+TG^- in α and δ phases, all trans(TTT) planar zigzag in β phase, and $T_3G^+T_3G^-$ in γ and ε phases. Thus, it would be very interesting if it is possible to obtain polar β phase directly from the solution casting method due to its advantages in easily to be modified and manufactured.

Few papers have reported fabrication of un-polarized β phase PVDF films from solution casting. PVDF films dissolved by hexamethylphoramide (HMPA) solutions were reported to have unoriented β phase crystalline structure.[9] Some authors described the method to get the γ phase using dimethylsulphoxide (DMSO) solution.[10-12] Solution-cast films of PVDF in dimethyl-formamide (DMF), and dimethylacetamide (DMAc) were reported to result in unoriented β phase transformation.[10, 12-13]

1.2. Research Objectives

Based upon many reasons described above, there is significant interest in supramolecular structure formation and there are needs in understanding of controlled-preparation of PVDF films using the solution casting method. This thesis will

report *in situ* corona poling with annealing of spin-casting PVDF and compare each sample from different conditions in respect of phase formation using wide angle x-ray diffraction and Infrared spectroscopy. We will also discuss about morphological, electrical and mechanical properties of solution casting PVDF films using Atomic Force Microscopy and Electrostatic Force Microscopy.

CHAPTER II

THEORIES AND PRINCIPLES

2.1. Chemistry of Poly(Vinylidene Fluoride)

Poly(Vinylidene fluoride) polymer has repeated monomer unit, $CH_2 = CF_2$, which is a gas at room temperature and pressure, and relatively stable.[4] Their physical, mechanical, thermal, electrical properties are found elsewhere. Table 1 shows basic and major properties of vinylidene fluoride monomer. The solubility of vinylidene fluoride is

Table 1 Properties of vinylidene fluoride.

Properties	Values
Chemical Formula	$CH_2 = CF_2$
Glass Transition Temperature	-38 °C
Melting Temperature	160 °C
Boiling Temperature	-86 °C
Freezing Temperature	-144 °C
Critical Pressure	4450 kPa
Critical Temperature	30 °C
Critical Density	0.416 g/mol
Amorphous Density at 25 °C	1.74 g/cm^3
Crystalline Density at 25 °C	2.00 g/cm^3
Molecular Weight	64.03 g/mol
Thermal Conductivity at 20 °C	0.723 m/K
Heat Capacity at 20 °C	13.6 cal/mol/K
Ionization Potential	10.3 eV
Dipole Moment	1.96 debye
Dielectric Constant	Min 5.6
Electrical Resistivity	10000 – 1.4e+016 ohm-cm
Dissipation Factor	0.05 - 0.37
Heat of Formation	-77.5 kcal/mol

less than 0.02g /100g of water at room temperature. The toxicity of vinylidene fluoride monomer is low, but care is taken for heating or melting of this polymer. Commercialsynthetic process of this polymer accompanies gaseous pyrolysis reactions. The preparation reactions of VDF are known by following chemical equation.

$$CF_3CH_3 \xrightarrow[\Delta]{} CH_2 = CF_2 + HF \qquad (11)$$

Poly(vinylidene fluoride) polymer is prepared by the polymerization reaction that is produced by addition of monomer to monomer unit.

$$n(CH_2 = CF_2) \xrightarrow{\text{catalyst}} -(CH_2CF_2)_n - \qquad \text{where} \quad n>1000 \qquad (12)$$

2.2. Phase Formation

There are at least five polymorphic forms of PVDF depending on the history of fabrication or polymerization. The three major chain conformations are shown by Figure 2

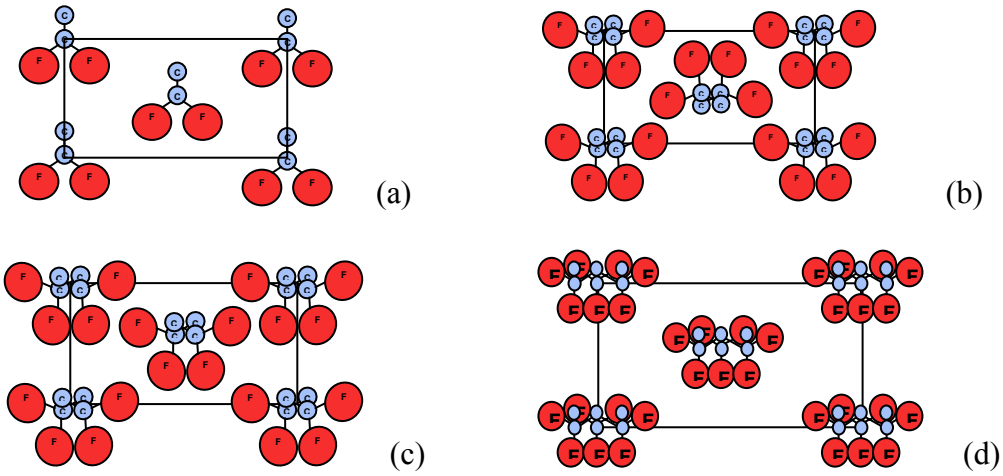

Figure 2 Four types of polymeric phase in PVDF crystal.

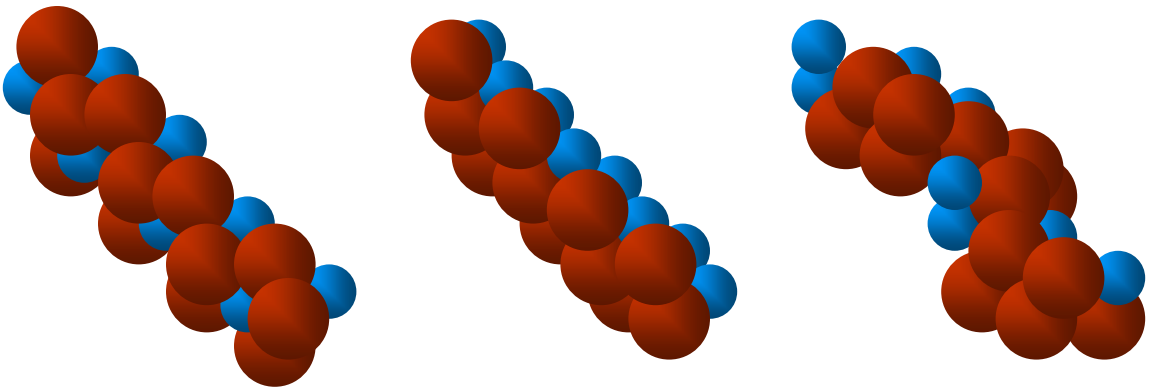

α $TGT\overline{G}$ β TTT γ $TTTGTTT\overline{G}$

Figure 3 Space filling models of PVDF in three conformations.

with omitting hydrogen. Figure 2 (a) is the crystal structure of beta phase (I), referred to as all-trans although successive -CF_2 groups must be deflected by about 7° in opposite directions from the planar zigzag conformation to accommodate the fluorine atoms.[14] It has piezoelectric properties better than most other piezo-materials, and is charged and aligned (Figure 3). The second picture (2b) shows $TGT\overline{G}$ structure of alpha phase (II) even though the bond rotations as deduced from the crystal structure are T=179° and G=45° rather than the ideal 180° and 60° respectively.[15] As one can see in Figure 3, Alpha is more homogenous. This enables it to be stable in nature and is non-polarized because of mixed positive and negative charges. The third one is referred to as delta phase (IV) or polar alpha phase made by the continuous electric field at the alpha phase form. The last one is gamma phase (III) with $TTTGTTT\overline{G}$ structure, has actual internal trans and gauche

rotation angles of about 170° and 52° respectively.[16] The polymer chains are transferred from alpha to beta phase when the films are stretched or rolled by deformation at below 100°C, or under continuous high electrical field. The beta phase has a net dipole moment and best piezoelectric coefficient after appropriate poling process. That is the reason there are many extensive works to make beta phase PVDF films.

2.3. Overview of Some Important Experimental Devices

2.3.1. Wide Angle X-ray Diffraction

Wide angle X-ray Diffraction (WAXD) is a widely used instrument to identify crystalline structure of polymers.[17-19] Their configurational determination of polymeric formation is highly dependent on time and data point. Diffracted angle of X-ray from surface can be defined by Bragg's Law (Figure 4),

$$n\lambda = 2d\sin\theta \tag{13}$$

where n is the order of a reflection, λ is the wavelength of X-ray, d is the distance between parallel lattice planes, and θ is the angle between the incident beam and a lattice plane.

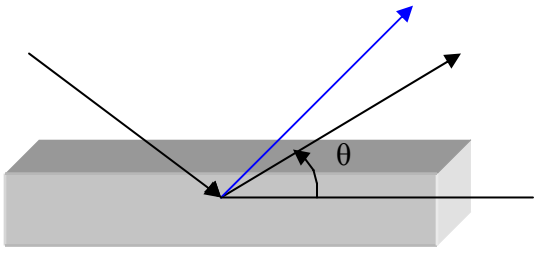

Figure 4 Principles of X-ray diffraction spectroscopy.

Result can be measured by value of intensity or count and it can be possible to determine crystallite size and size distribution.

2.3.2. Fourier Transform Infrared Spectroscopy

Fourier Transform Infrared Spectroscopy is useful for determining routine organic structures by using absorption, transmission, and diffraction of infrared wave.[10-11, 20] IR range is valid from the red end of the visible region to the microwave region at the low frequency. It makes it possible to use for the sample thickness from 2.5 to 15 μm corresponds to approximately 4000 to 600 cm^{-1}. The polymer molecules will absorb the radiation from the infrared wave when the frequency of specific molecular vibration of materials is coincided with the frequency of incident radiation of specific vibration. The characteristic stretching frequency (cm^{-1}) of two atoms of masses m_1 and m_2 can be detected by following equations,

$$\nu = \frac{1}{2\pi c}\sqrt{\frac{k}{\mu}} \tag{14}$$

where k is force constant, $\mu = m_1 m_2/(m_1+m_2)$, and c is the velocity of light. Nowadays, Fast Fourier Transform makes it possible to scan very fast and can save the time.

2.3.3. Atomic Force Microscopy

An Atomic Force Microscope is the one of the most innovative microscopes to measure the topology, phase, and many useful surfaces and material properties. It was done using probes with few nm size of radius in the bottom. In addition, there are many extensive applications such as making patterns on the surfaces, modifying the surfaces and manipulating bio-, nano-materials.[21-23] Their resolution is extremely high, for

example, STM (Scanning Tunneling Microscopy) with vacuum chamber has a few nm in resolution. Figure 5 shows schematic diagram measuring surface topography using an Atomic Force microscope. The signal change from laser movement due to the cantilever movement or vibration can be detected by photo diode sensor when the probe travels the sample surface. Through the feedback loop, this signal change will be imaged by software. There are two major types of scanning modes, which are contact and close contact (or tapping mode). The contact mode AFM is useful to make clear topography image for the hard materials with low average roughness rather than soft ones. They can make the

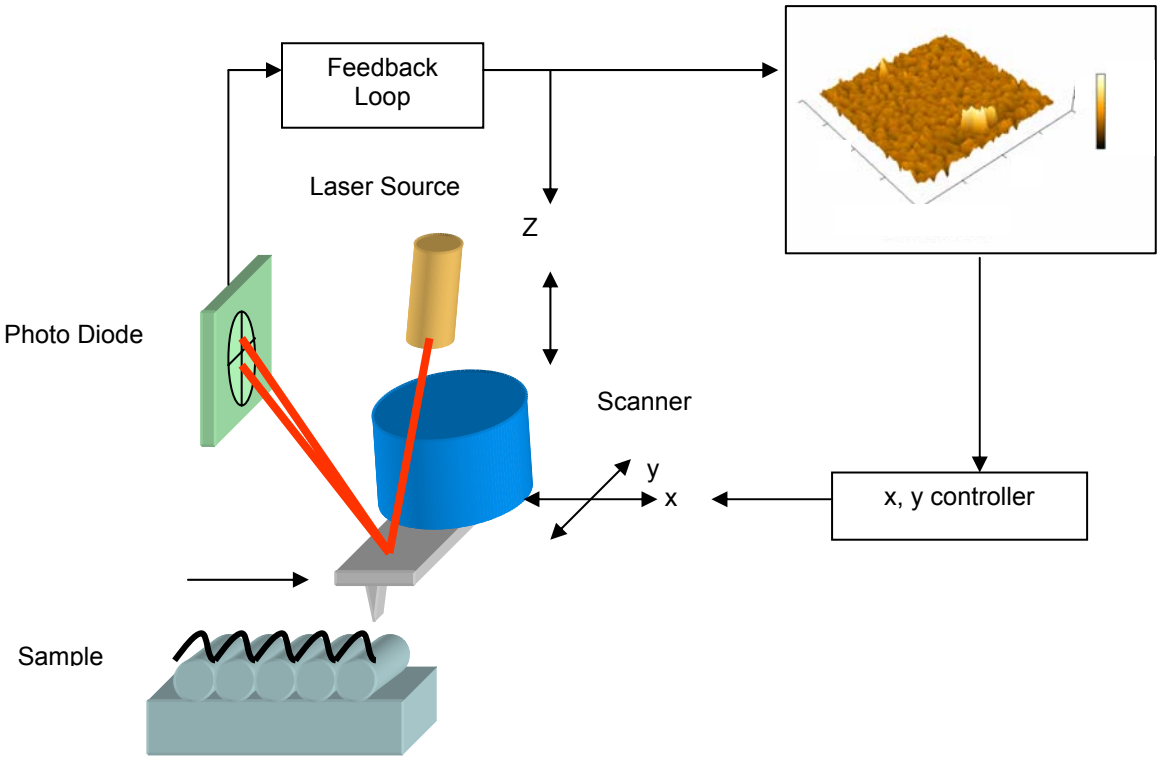

Figure 5 A schematic diagram of AFM operation.

surface of soft materials change or destroy because they always contact with sample surface on the scanning. Because of their characteristics that contact with surface, this mode is useful to measure the friction or adhesion force by sensing the left, right deflection of the probe on the scanning. Adhesion force can be measured by the force displacement curve on contact mode. Figure 6 shows principles of measurement of adhesion force, that probe is approaching from A to C with increasing attraction force and detaching from C to D because of existence of repulsive force with causing sudden pull off from D to E. The distance between B and D is caused by adhesion force. Adhesion force can easily calculated by Newton's Law.

$$F_{Adhesion} = k \times \Delta x \tag{15}$$

where k is spring constant (nN/nm) of the AFM probe. Friction force can be measured by roughness average of left, right deflection due to the friction coefficient. Close contact mode or tapping mode is useful for phase change detection and non-destructive imaging. Tapping mode eliminates the problems associated with friction, adhesion, electrostatic forces due to the surface contact on the scanning. Tapping mode imaging uses oscillating of the cantilever assembly at or near the cantilever's resonant frequency at ambient air. The oscillating tip approaches to the surface until it begins to lightly touch the surface. When the oscillating cantilever begins to contact the surface, the change of cantilever oscillation is detected for identifying and measuring surface features. Tapping mode makes it possible to measure the topography and phase of soft materials without any destruction because they oscillate at very high frequency (about 200 kHz) with low amplitude.

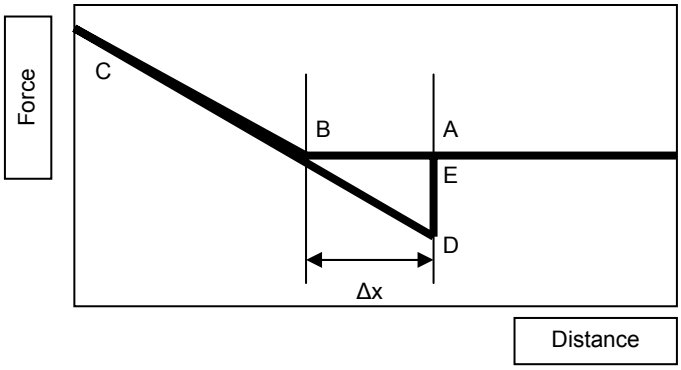

(a) Force-displacement curve.

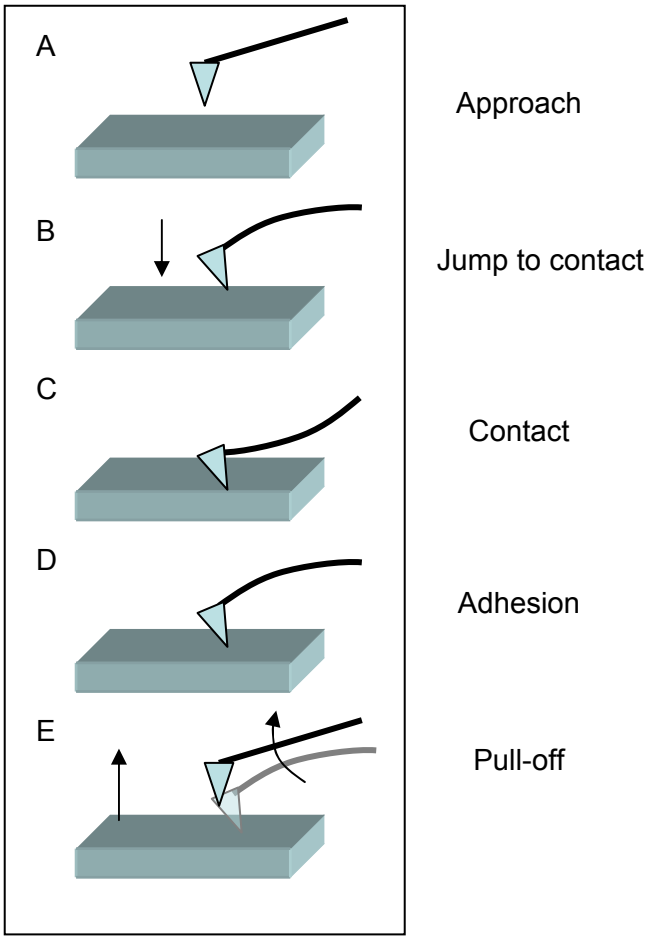

(b) Movement of cantilever.

Figure 6 A schematic diagram of measuring adhesion force.

2.3.4. Corona Discharger

Unpolarized PVDF films do not usually make large piezoelectric coefficients because their dipole moment is not aligned. The corona discharging is one of the powerful methods of PVDF polarization.[24-25] Corona is self persistent electrical discharge in a gas where the Laplacian electric field limits the primary ionization process to regions near to high field electrodes.[26] The poling process can be completed in several seconds at room temperature.[27-28] Corona polarization is able to acquire continuous higher fields than other polarization methods.

CHAPTER III

EXPERIMENT

3.1. Film Preparation

3.1.1. Cleaning Substrate

Silicon wafers were carefully cut by diamond tip, and cleaned with Pirahna and HF solution each for removing silicon oxide and organics for a few minutes. After that, they were rinsed with DI water and isopropyl alcohol, acetone for 5min each, and dried with N_2 gas step by step at clean environment (Class 1000).

3.1.2. Gold Deposition

Gold as a bottom electrode for piezoelectric thinfilms was deposited on the silicon substrate using vapor deposition system. They were deposited at 15mA at 100 mili-torr for 7 min. This would lead to a film thickness of 100nm.

3.1.3. PVDF Solution Preparation

Granular type PVDF was supplied by Goodfellow Inc. (Cambridge, England). PVDF solvent dimethylsulphoxide (DMSO) and chemicals were used as received from EMD chemicals Inc (USA). The acetone (80 ml) and DMSO (20 ml) solution were added to all the PVDF. The PVDF concentration was 40g/L, 60g/L, 80g/L, and 100g/L each for various viscosities. Hotplate with stir was prepared at 40°C to dissolve them fast. It takes 30min~40min to dissolve PVDF completely.

3.1.4. Film Casting

The different viscosities of PVDF solutions were coated on the gold-silicon

substrate using spin coater (SCS P6204) with various spin speed. The films were baked by controlled hotplate at various temperatures during before and after 30min with *in situ* corona poling at 30kV for 2min (DB-20AC, electro technic products Inc.).

3.2. Film Analysis and Image Measurement

Both wide angle x-ray diffraction (D8 Advance, Bruker Axs Inc., USA) and FTIR were used for checking the phase of all the samples. Each scan was performed with wide angle x-ray diffraction with 2θ angle ranging from 10 to 70° and a chopper increment of 0.04°. FTIR spectra were obtained in the wave number range of 200-1600 cm^{-1} to enforce their validity comparing with WAXD. Using these two methods, phase formation of each

Table 2 PVDF crystal phases and their corresponding values.

Phase	**WAXD** **2θ (°)**	FTIR bands (cm^{-1})
α phase	**17.7, 18.4, 19.9, 27.8, 35.7, 39, 57.4**	532, 612, 763, 796, 854, 870, 970, 974, 1210, 1383, 1423
β phase	**20.7, 20.8, 35, 36.6, 56.1**	510, 839, 1286, 1431
γ phase	18.5, 19.2, 20.1, 20.3, 26.8, 36.2, 38.7	812, 882, 1234

sample could be verified eliminating uncertainty of dubious data peak. Table 2 shows reference data for these two methods. The thickness and roughness of films were identified by profilometry (Dektak3, Veeco Instrument, USA). Topology and phase image of each films were observed by using an Atomic Force Microscope (Nano-R, Pacific Nanotechnology Inc., USA, ref. Figure 7). The nano-scale roughness data were also acquired by on the same scan. Adhesion force in nano-scale through force distance curve and Friction mode of LFM (Lateral Force Microscopy) were calculated by equation 15. Friction forces were compared with each other from average values through L-R mode. Electrostatic force images were obtained for observing the electrical phase change due to electrical force gradients from the samples using Electrostatic Force Microscopy (Nanoscope IIIa, Veeco, USA).

Figure 7 Atomic force microscope (Nano-R, Pacific Nanotechnology Inc., USA).

CHAPTER IV

RESULTS AND DISCUSSION

4.1. Film Thickness and Roughness

It is important to measure the thickness and roughness of PVDF films from different conditions such as spin speed and viscosity for satisfying desired specifications of films with respect of both experimental uses and applications. Film thicknesses can be measured using profilometer by carefully cutting small part of films and measuring the height difference. The roughness of films was measured by using both an Atomic Force Microscope and a profilometer. A certain roughness value is desirable for stable mechanical, electrical, and material properties. An AFM can conduct measurement in nanoscale. Figure 8 shows the thickness and roughness of films as a function of spin speed and viscosity with same spinning time for 30s. It is obvious to get thicker films as the spin speed decreases and the viscosity increases. The thickness and roughness values fluctuate at values less than 500rpm because of their un-stability of spinning motion. It shows more stable trends for both values at high spin speed. In case of the roughness, it is also dependent on their thermal conductivity. Non-uniformed heat could cause some porous on the PVDF films due to solvent evaporation. Figure 9 presents AFM topography image, phase image, and their roughness analysis of the sample surface with spin speed 500rpm at 40g/L solution. The phase image of AFM can give some information about contamination of sample surface. The image proves less contamination of sample surface. The roughness

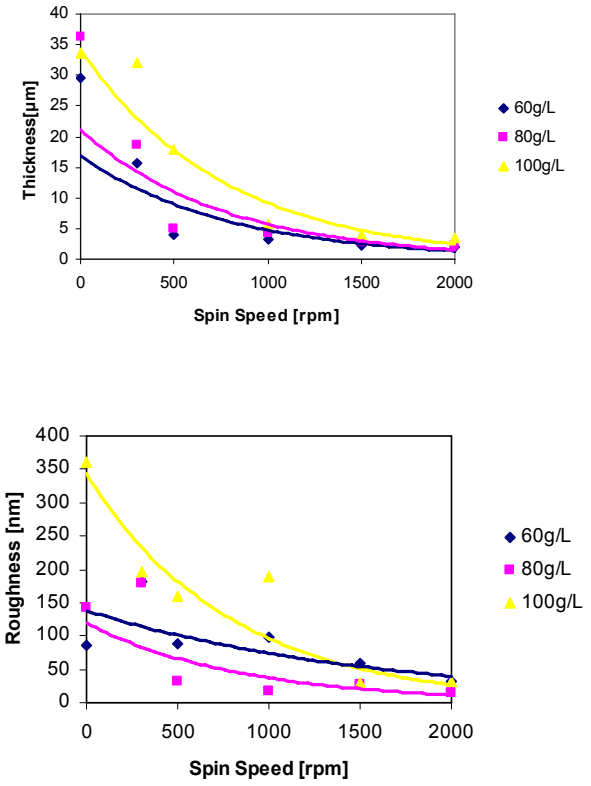

Figure 8 Plot of thickness and roughness with different viscosities vs spin speed.

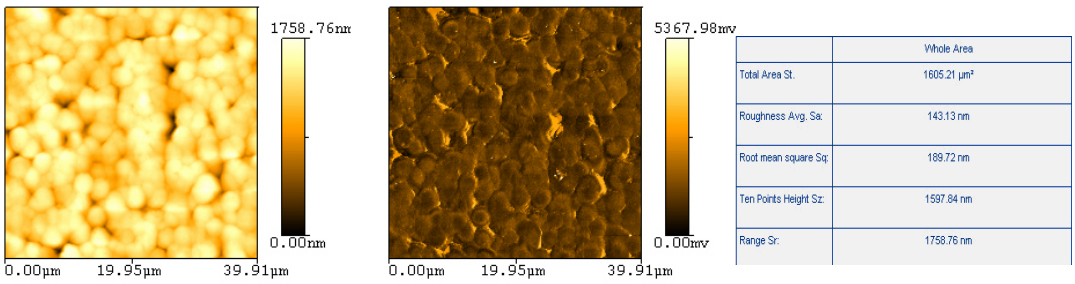

Figure 9 Topography and phase image and roughness analysis of a sample with spin speed 500rpm at 40g/L.

values of samples using AFM and those of profilometer provides a good agreement.

4.2. Wide Angle X-ray Diffraction and FTIR Spectra

The polymeric phase of solution-cast PVDF film with different conditions was studied by both wide angle x-ray diffraction and FTIR method. These two methods have been commonly used for phase identification of for several years.[10-11, 20] It is difficult to define the phase of films implicitly due to ambiguity of values occasionally. It is because of in-appropriate leveling of samples that can leads to transform their peak value to incorrect Bragg angle and interferences of substrate material that can provide some trivial peak information. Thus, it gives good compromise to compare the data from these two methods. Samples on the cleaned silicon substrate with gold coating were prepared by spin coating method at 3000rpm for 30s with viscosity of 80g/L. Samples were then annealed at room temperature (23°C), 40°C, 60°C and 80°C with corona poling of 30kV for 2 min. Figure 10 shows X-ray diffraction data for a change in the crystallinity of each sample. It is shown clearly that all samples have strong peaks near to 38°, which represent γ phase. This γ phase peaks are weak in Samples C and D. No more information was given from this X-ray diffraction patterns because these peaks are to close to each other. Nevertheless, the X-ray method provided useful information that crystallines do indeed include γ phase on them. Results from the Infrared Spectroscopy analysis of the same samples are shown in Figure 11. It is clearly shown that peaks of γ and β phases from the sample A, B, C, and D at 840, 1286, 1430 for β phase and at 880, 1234 for γ phase. The β phase peak decreases and γ phase peak increases as the temperature of annealing increases. In case of sample C and D, the annealing temperatures were so high that their

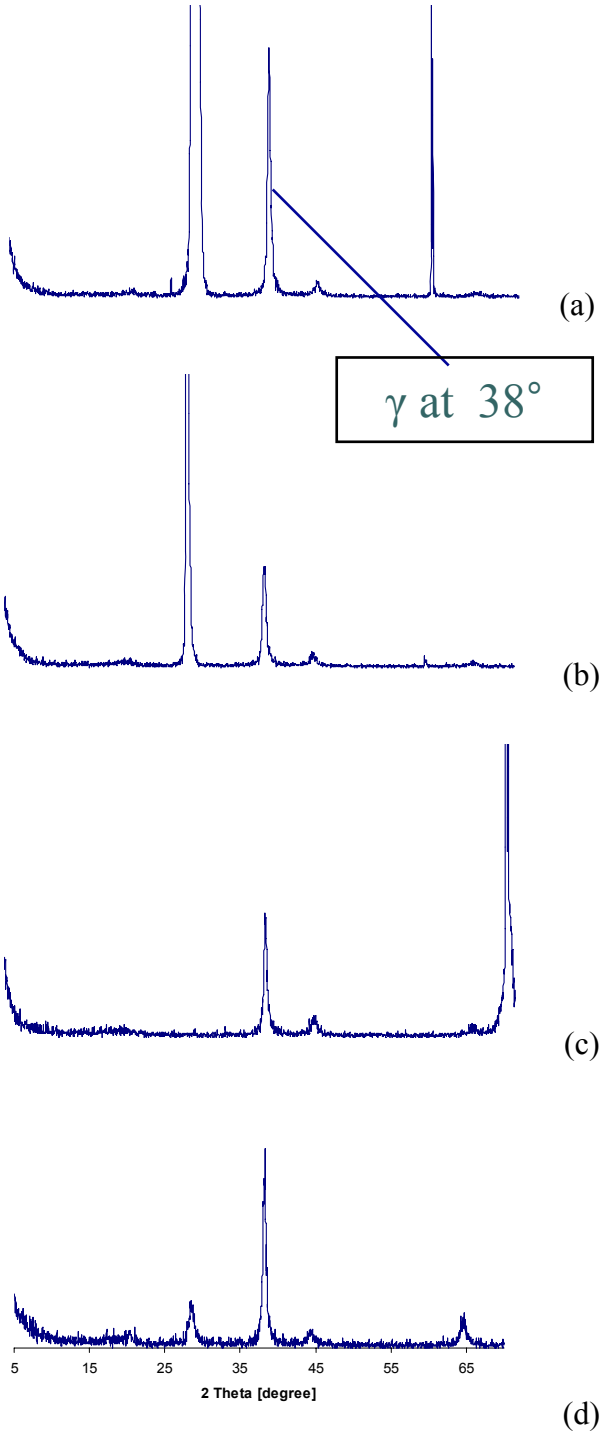

Figure 10 X-ray diffraction data for sample A-D.

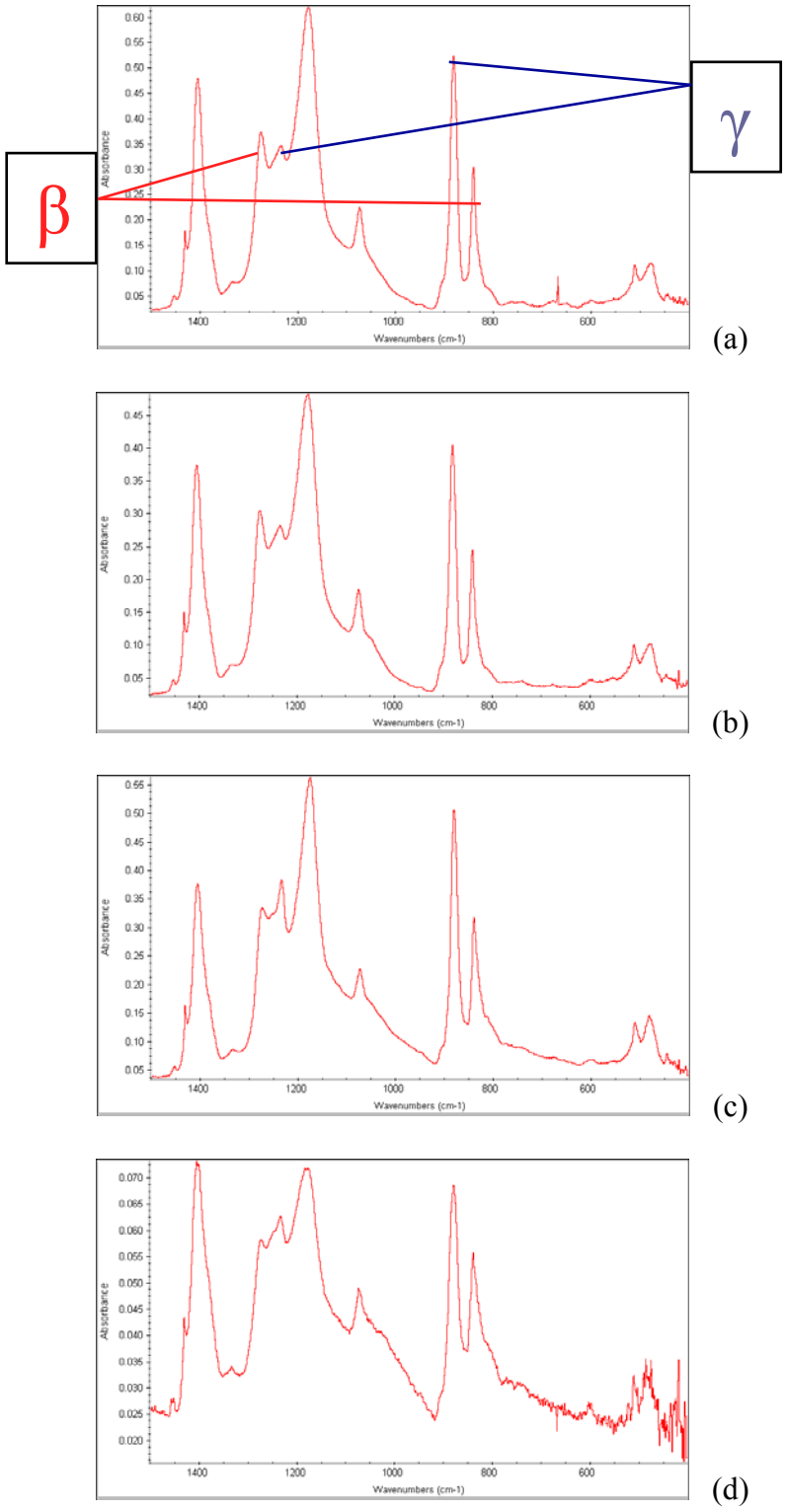

Figure 11 FTIR data for sample A-D.

solvent evaporation rate was rather fast. This eliminates the possibility aligning polymer chains. That is the reason there are more γ phase in samples c and d than samples a and b.

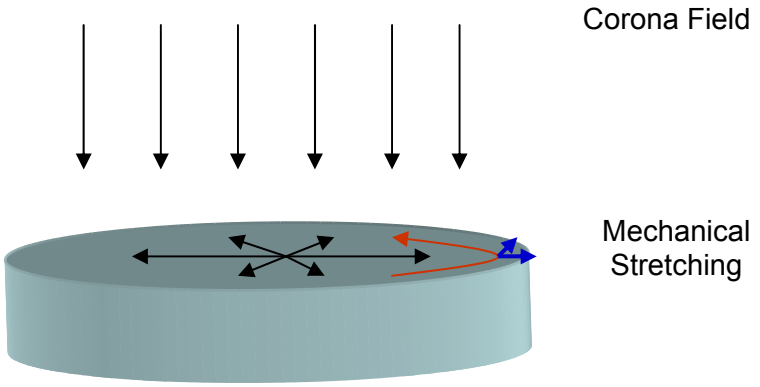

(a) Overview of experimental system.

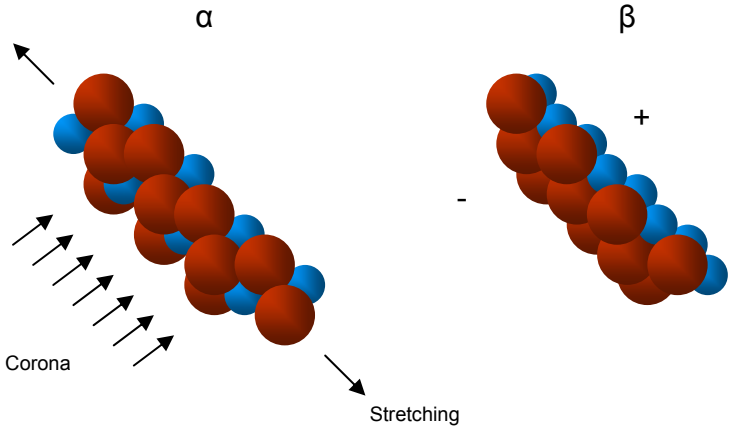

(b) A schematic diagram of chain transformation.

Figure 12 A schematic diagram of in-situ corona poling with spin coating.

The γ phase has similar packing with α phase. The schematic diagram illustrates the conceptual idea shown in Figure 12. Instead of mechanical stretching, spinning motion and heating trigger the change of chain packing and *in situ* corona poling provides a chance of dipole alignment. It is also important to use polar solvent such as DMSO, and DMAc for helping crystal alignment from their polar properties.

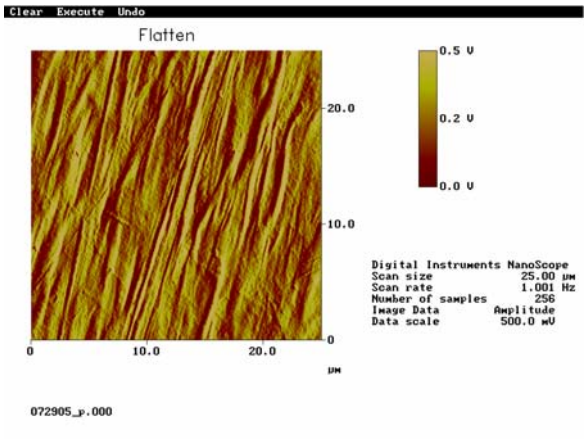

(a) Phase image of commercial PVDF thin film.

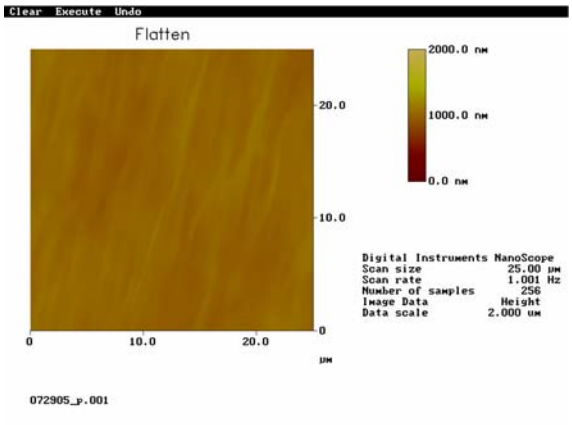

(b) EFM image of commercial PVDF thin film.

Figure 13 EFM image of commercial PVDF thin film with thickness 52 μm.

4.3. Atomic Force Microscope Measurement

The morphology and phase images were obtained using an Atomic Force Microscope. Images are compared with each other in the following. Before this measurement, EFM image of commercial sample are investigated first. This commercial sample is a PVDF thinfilm that was uniaxially oriented and polled with a thickness of 52 μm (provided by the Measurement Specialties, Inc.). The dielectric property and the orientation of the film were tested using the EFM (DI Nanoscope IIIa). It is seen that the structural pattern were mechanically stretched and orientated (Figure 13a). The Electrical phase change due to electrical force gradients from the sample are seen in Figure 13b. Electrical phase change is uniform that provides a stable electrical charge for certain practical applications. Some morphological images that are considered as a trace of similar orientation or equivalent mechanical stretching comparing with commercial sample were observed using AFM

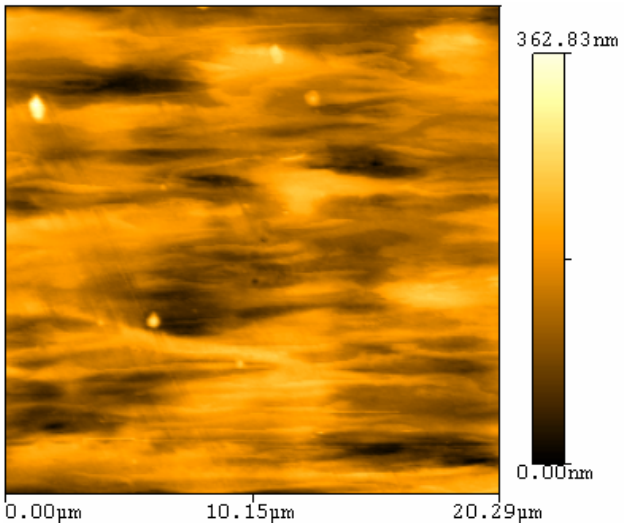

Figure 14 Stretching of PVDF film triggered by high spinning motion.

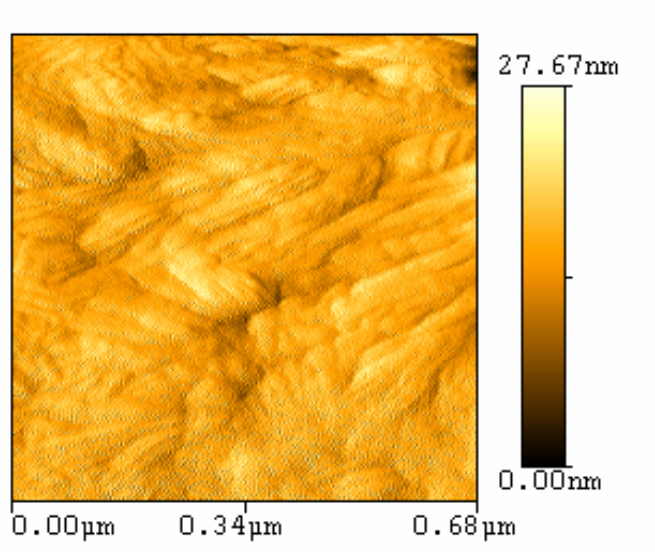

Figure 15 Biaxial stretching of PVDF film in nano-scale.

from the high speed spin coating (3000rpm). As one can see from Figure 14, stretching direction is horizontal and their spherulites and fibers connected from one spherulite to another can be observed. This picture further confirms the result in Figure 13a where mechanical stretching promotes chain alignment. An interesting AFM image is shown in Figure 15 indicating nano-scale stretching from small area image. Their stretching direction seems to be two, which are radial and tangential to the spinning motion.

The sample A which has mixture of γ and β phase (verified by FTIR analysis) was analyzed using an AFM. It is seen that there are at least two different morphological patterns in Figure 16. One is white and the other is dark. If one looks into smaller scale, one sees totally different structures of surface morphology. Figure 17 shows some useful information regarding this. The center part of this phase image seems to be different with

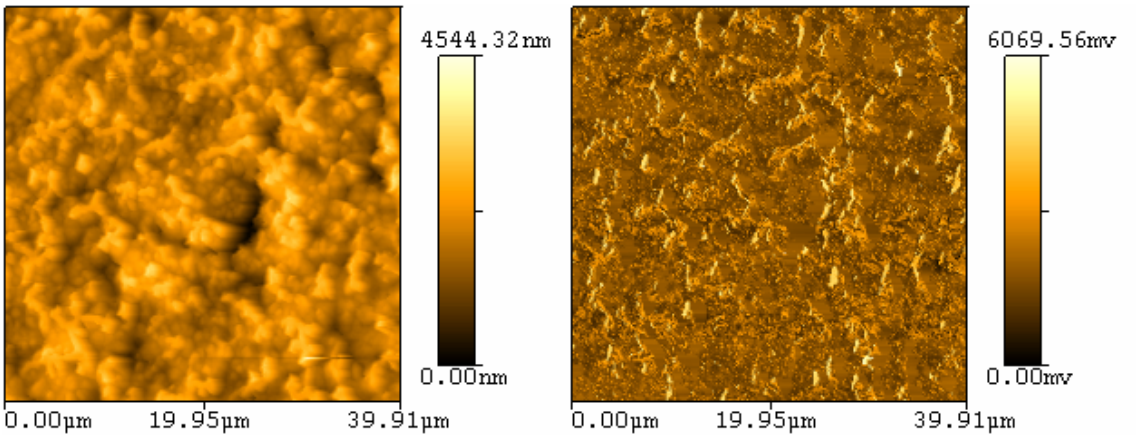

Figure 16 Topography (left) and phase (right) image of sample A in 40µm.

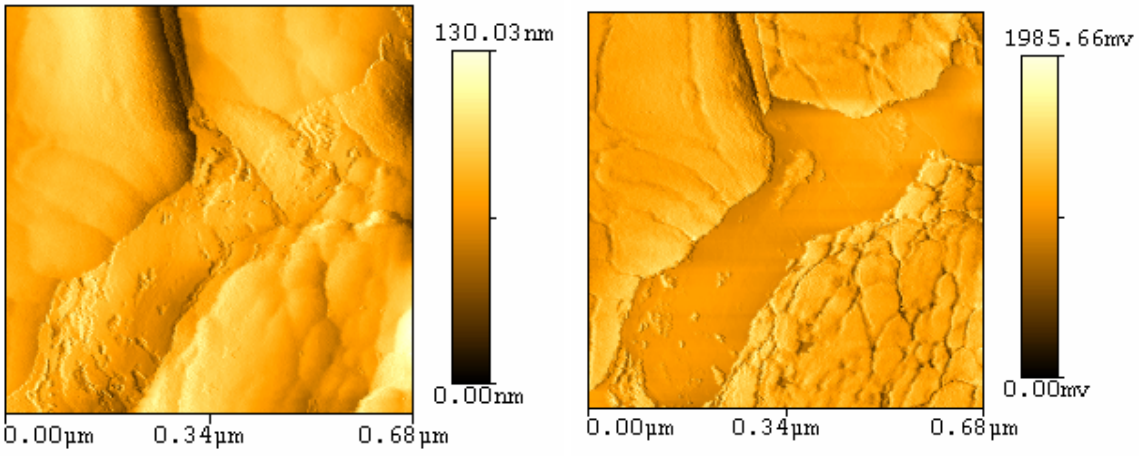

Figure 17 Topography (left) and phase (right) image of sample A in 680nm.

upper and bottom one morphologically. It is not known which one is γ or β, or even α phase. There is no literature about this. Nevertheless, this image can be useful to understand supramolecular behavior of PVDF in future research. For the comparison of α, γ, or β phase, it is imaged for the sample to be identified as almost α phase. It is seen that

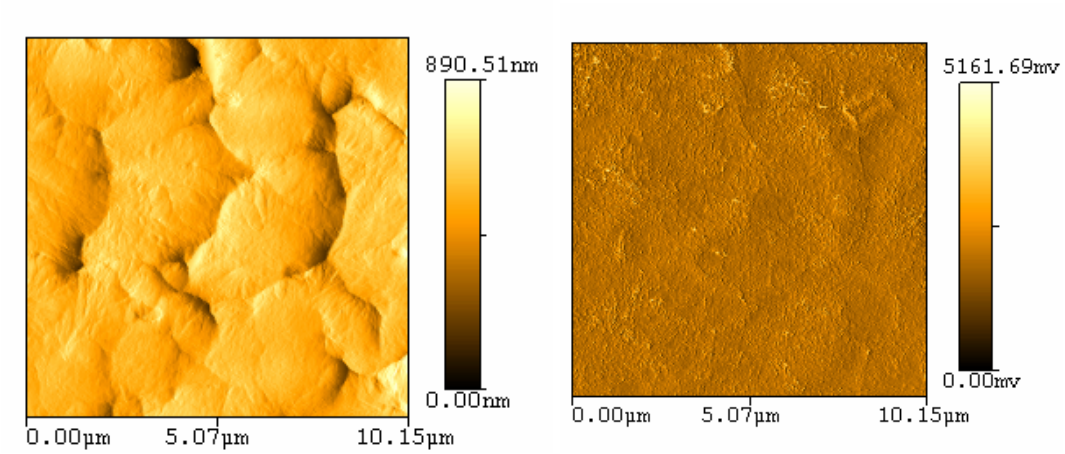

Figure 18 Topography (left) and phase (right) image of α phase sample.

this sample has only one type of polymer structure (Figure 18).

Nano-scale adhesion and friction of sample A, B, C, and D are defined by Lateral Force Microscopy. It is important to investigate micro-, nano- scale adhesion and friction force for MEMS or NEMS application as a PVDF sensor or actuator. For the MEMS or NEMS parts, friction and adhesion can destroy their connection among the parts and stop their operation through whole devices because of their low energy to operate systems, small clearance between each part, and high surface area ratio comparing with their volume.[29-31] Based on the described theory from chapter III, adhesion force is measured by LFM. For example, sample A can be measured by equation $F_{Adhesion} = k \times \Delta x$ =1.8(nN/nm) ×310.96nm=732.6nN, where k is force constant of cantilever, 1.8nN/nm (Figure 19). Comparison chart of the adhesion force for each sample be displayed by Figure 20. From the chart, the adhesion force of α and mixture of β and γ are almost same,

Figure 19 Force displacement curve of sample A.

but sample D has high adhesion force, which is more γ phase than others. It is reasonable to think that the amount of β phase reduces adhesion force due to their electro-static force. Gripped by tweezers or other materials, β phase sample is less electrostatic than that of γ or α. Nonpolar α phase sample has also high adhesion force. It is considered because of the effect of electrostatic force. The existence of high electrostatic force from non polar alpha phase can be observed through naked eyes. Friction values of samples were investigated by using the L-R deflection mode of LFM. Figure 21 plotted comparison of friction values. It shows very high friction value for sample A and B which have high β phase contents. The β phase content lead to a high roughness value comparing with samples with almost pure phased one. That is why mixture of different phases increases the friction and

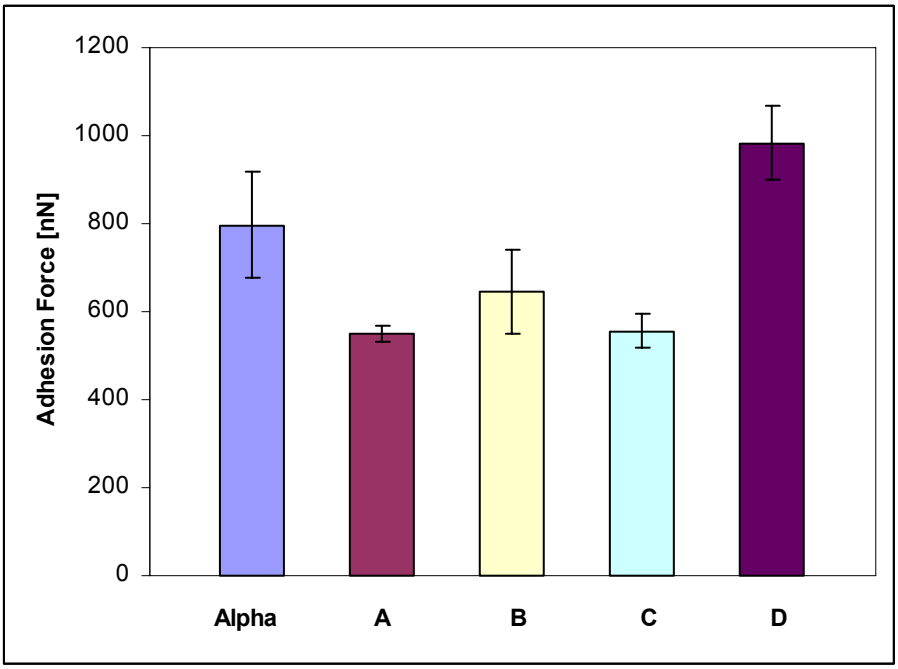

Figure 20 Plot of adhesion force of samples.

roughness values. In conclusion, a sample with pure beta phase has either low adhesion or friction value. For sensing materials, electrostatic and adhesion can be more important. For actuating, friction will be one of the main concerns. We can compromise between these two factors. Further study on friction and adhesion force in nano-scale among different phases is recommended. There is challenges in studying nano- scale adhesion and friction force of different phase samples with same roughness through Polymer CMP(Chemical Mechanical Planarization).

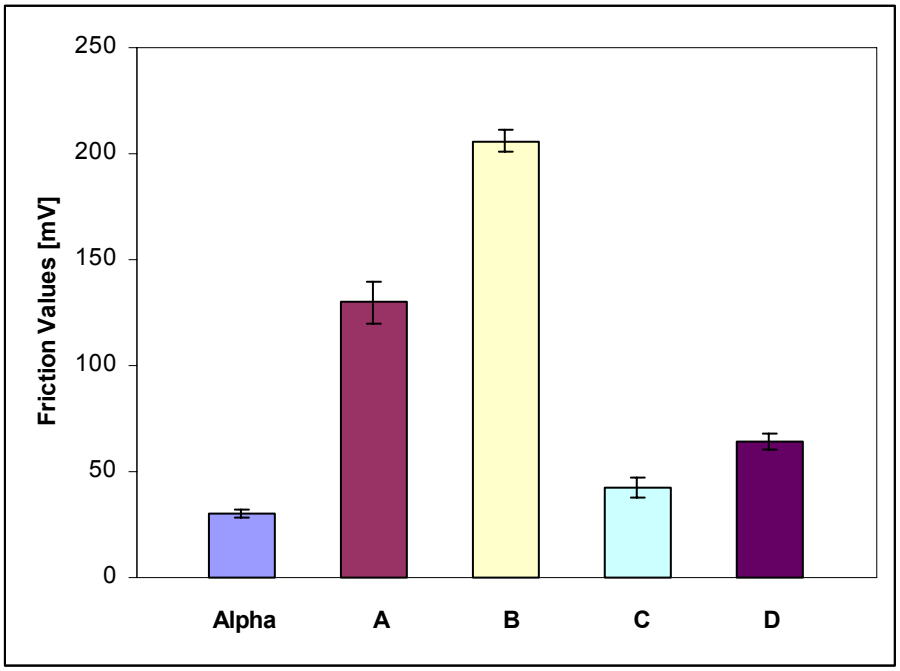

Figure 21 Plot of friction value of samples.

CHAPTER V

CONCLUSIONS AND REMARKS

5.1. Conclusions

PVDF polymer and their properties, phase conformation, and analytical methods were reviewed at the beginning of this thesis. The thinfilms of poly(vinylidene fluoride) were fabricated using the spin coating method from solution of PVDF and polar solvent DMSO with different thermal conditions with *in situ* corona poling and annealing. Based on the X-ray diffraction and FTIR analysis, these films have conformational phase change from α to mixture of β and γ phase. This process can decrease the complexity of the conventional method which requires mechanical stretching before poling of PVDF in addition to thermal annealing for β phase transformation. Depending on the thermal annealing, phase change was different. If the annealing temperature is high, their solvent evaporation rate was fast leading to lack of time to align polymer chains. Instead of mechanical stretching, spinning motion and heating trigger the change of chain packing and *in situ* corona poling provided proper alignment.

According to the AFM topography and phase image, there were at least two different morphological patterns in the sample. On the other hand, it was observed for pure α phase sample to have only one morphological image. The adhesion force, friction force was measured by using the LFM. The β phase contents decreased adhesion force because the electrostatic force in β phase was less than that of α or γ, and a pure phase decreased friction values and roughness.

This research presented the nano-characterization of polymers for the first time to link microstructures with surface forces (friction and adhesion, etc.) It opens areas of future investigation.

5.2. Suggested Future Research

The following topic and contents are suggested for future study:

- The size effect of piezoelectric polymer can be studied by micro- and nano-scale patterning of PVDF sample. The surface area ratio of sample dimension can affect their piezoelectric response.
- The friction and adhesion force of PVDF film can be studied in detail according to phase difference. This needs techniques for polymer CMP (Chemical Mechanical Planarization) in order to control roughness values.
- To improve their orientation and polarization properties of PVDF, mixtures of other polymers, copolymers, can be fabricated and studied by using specialized analytical techniques.
- Morphological behavior of PVDF film due to the heat treatment and humidity control can be extensively studied using *in situ* observation using AFM. This research needs techniques for thermal and humidity control.

REFERENCES

[1] G. Gautschi, *Piezoelectric Sensorics*, Springer, Berlin, (2002).

[2] G.W. Taylor, J.J. Gagnepain, T.R. Meeker, T. Nakamura, and L.A. Shuvalov, *Piezoelectricity*, Gordon and Breach Science Publishers, New York, (1985).

[3] T. Ikeda, *Fundamentals of Piezoelectricity*, Oxford University Press, Oxford, (1990).

[4] T.T. Wang, J.M. Herbert, and A.M. Glass, *The Applications of Ferroelectric Polymer*, Blackie, New York, (1988).

[5] M. Yoo, C.W. Frank, S. Mori, and S. Yamaguchi, *Chem. Mater.,* **16***,* 1945-1953, (2004).

[6] A. Arnau, *Piezoelectric Transducers and Applications*, Springer, Berlin, (2004).

[7] J. Singh, *Smart Electronic Materials*, Cambridge University Press, Cambridge, (2005).

[8] A.S. Bhalla, K.M. Nair, I.K. Lloyd, H. Yanagida, and D.A. Payne, *Ferroic Materials: Design, Preparation, and Characteristics*, Ceramic Transactions, Westerville, OH, (1994).

[9] M. Kobayashi, and K. Tashire, *Macromolecules,* **8**, 158, **(**1975).

[10] M. Benz, W.B. Euler, and O.J. Gregory, *Macromolecules***, 35***,* 2682-2688, (2002).

[11] A. Salimi, and A.A. Yousefi, *J Polym Sci Part B: Polym Phys*, **42**, 3487–3495, (2004).

[12] R. Gregorio, and M. Cestari, *J. Polym Sci*, **32**, 859, (1994).

[13] D.T. Grubb, and K.W. Choi, *J Appl Phys*, **52**, 5908, (1981).

[14] R. Hasegawa, Y. Takahashi, Y. Chatani, and H.Tadakoro, *Polymer J*, **2**, 600, (1972).

[15] M.A. Bachman and J.B. Lando, *Macromolecules*, **14**, 40, (1981).

[16] S. Weinhold, M.H. Litt, and J.B. Lando, *Macromolecules*, **13**, 1178, (1980).

[17] D.M. Esterly, B.J. love, *J Polym Sci Part B: Polym Phys,* **42**, 91–97, (2004).

[18] G. Laroche, C. Lafrance, R.E. Prud'homme, and R. Guidoin, *J Biomed Mater Res,* **39,** 184–189, (1998).

[19] G.A. Maier, G. Wallner, R.W. Lang, and P. Fratzl, *Macromolecules***, 38***,* 6099-6105, (2005).

[20] E. Benedetti, S. Catanorchip, A. D'Alessio, G. Moggi, P. Vergamini, M. Pracellad, and F. Ciardelli**,** *Polymer International,* **41**, 35-41, (1996).

[21] J. Shiracashi, K. Matsumoto, N. Miura, and M. Konagai, *Jpn J Appl Phys*, **36**, 1257-1260, (1997).

[22] D. Foriadis, S. Scheuring, and S. A. Muller, *Micron*, **33**, 385-397, (2002).

[23] D. Anselmetti, J. Friz, B. Smith, *Single Mol*, **1**, 53-58, (2000).

[24] J. Sinézio Cavalho Campos, *Rev Sci Instrum*, **61**, 1143-1150, (1990).

[25] D.K. Das-Gupta, and K. Doughty, *J Phys D: Appl Phys*, **11**, 2415-2423, (1978).

[26] M.I. Akcan, and C. Topacli, *Polym Int,* **50**, 835-840, (2001).

[27] P.D. Southgate, *Appl Phys Lett*, **28**, 250, (1976).

[28] T. Tominaga and K. Fukunaga, Japan Pat 74-83899, *Chem Abstr*, **82**, (1975).

[29] Y.C. Tai, L.S. Fan, and R.S. Muller, *Proc. IEEE MEMS*, **89**, 1-6, (1989).

[30] K. Deng, R.J. Collins, M. Mehregany and, C.N. Sukenik, in *Proc. MEMS 95*, Amsterdam, Netherlands, (Jan-Feb 1995).

[31] W.S. Trimmer, *Micromechanics and MEMS, Classic and Seminal Papers to 1990*, IEEE Press, New York, (1996).

VITA

TAE KWON JEE

4302 College Main APT 107, Bryan, TX, 77801

Email: sreilike@tamu.edu

Education

Texas A&M University, College Station, Texas, USA

Master of Science in Mechanical Engineering, 12.2005

Hanyang University, Seoul, Korea

Bachelor of Science in Mechanical Engineering, 02.2004

Experience

Surface Science Lab**, Texas A&M University,** College Station, Texas, USA

Research Assistant, 06.2005-current

Applied Tribology Lab**, Korean Institute of Science and Technology,** Seoul, Korea

Commissioned Research Scientist, 06.2003~06.2004

Research Project

"*Fabrication of micro piezoelectric sensor*", sponsored by the National Science Foundation (IIS-0515930). Advisor Dr. Hong Liang, 02.2005-current

"*Development of nanoscale manipulation system*", sponsored by the Center for Nano-scale Mechatronics and Manufacturing and the Korean Ministry of Science and Technology. Advisor Dr. Euisung Yoon, 2003-2004